Research Article | Vol. 12, No. 11 / 1 Nov 2021 / Biomedical Optics Express 7139
Biomedical Optics EXPRESS

Low-consumption photoacoustic method to measure liquid viscosity

YINGYING ZHOU,[1,2,3,6] CHAO LIU,[1,6] XIAZI HUANG,[2,3,6] XIANG QIAN,[4] LIDAI WANG,[1,5,7] AND PUXIANG LAI[2,3,8]

[1]*Department of Biomedical Engineering, City University of Hong Kong, Hong Kong*
[2]*Department of Biomedical Engineering, Hong Kong Polytechnic University, Hong Kong*
[3]*The Hong Kong Polytechnic University Shenzhen Research Institute, Shenzhen, China*
[4]*Tsinghua-Shenzhen International Graduate School, Tsinghua University, Shenzhen, China*
[5]*City University of Hong Kong Shenzhen Research Institute, Shenzhen, China*
[6]*These authors contributed equally to this work*
[7]*lidawang@cityu.edu.hk*
[8]*puxiang.lai@polyu.edu.hk*

Abstract: Viscosity measurement is important in many areas of biomedicine and industry. Traditional viscometers are usually time-consuming and require huge sample volumes. Microfluidic viscometry may overcome the challenge of large sample consumption but suffers from a long process time and a complicated structure design and interaction. Here, we present a photoacoustic method that measures the liquid viscosity in a simple microfluidic-based tube. This new viscosity measurement method embraces fast detection speed and low fluid consumption, offering a new tool for efficient and convenient liquid viscosity measurement in a broad range of applications.

1. Introduction

Measurement of viscosity, an important thermophysical property, plays a key role in material characterization in many fields of biomedicine and industry [1,2]. For example, blood viscosity is an important clinical parameter due to its close tie with cardiovascular diseases [1,3,4]. The oil viscosity is one of the most important parameters to evaluate the automotive engine oil conditions [2]. Various methods have been developed to determine the liquid viscosity. Conventional viscometer usually takes a long time and consumes a large volume of liquid for accurate measurement. For example, it may take ~1 mL amount and up to ~1 hour for one measurement, which is not ideal for frequent monitoring or when samples are precious or scarce [5–7]. To reduce sample consumption and increase the efficiency, microfluidic methods have been developed in recent years, where the sample consumption has been reduced to hundreds of microliters. For example, Lan *et al.* designed a co-axial microfluidic device to measure the Newtonian fluid viscosity, which allows for a stable liquid/liquid annular co-laminar flow measurement based on Navier-Stokes equations [8]. Kim *et al.* proposed to deliver the sample and reference fluids separately into two inlets of a Y-shaped microfluidic device so that one can measure the sample viscosity by measuring the interfacial width, which is induced at the downstream of the Y-shaped device [9]. Kang *et al.* demonstrated a high-precision microfluidic viscometer with a microfluidic channel array composed of 100 indicating channels using only ~100 µL sample [10]. These methods have significantly reduced the sample consumption, but the supporting microstructure of the device needs to be specifically designed in advance, which is usually complex, costly, and time-consuming. Moreover, the compatibility relies heavily on the interaction between the microstructure and the test sample. That is, for different types of samples, one may need to design different supporting microstructures, which further tightens the requirements and increases the design complexity and operation cost [11]. Therefore, to broaden the application of microfluidic-based viscosity measurement to more labs and to make

#444144 https://doi.org/10.1364/BOE.444144
Journal © 2021 Received 23 Sep 2021; revised 17 Oct 2021; accepted 19 Oct 2021; published 27 Oct 2021

Biomedical Optics EXPRESS

blood viscometry available for frequent testing, there is an urgent need for a high-speed, low dose consuming, and precise viscosity measurement method that can be used in a broad range of generic microfluidic-based channels.

Photoacoustic (PA) tomography is a new imaging technique that has been developed for a wide range of applications [12–22], including liquid viscosity measurement. For example, in 2010 Lou *et al.* proposed to use the frequency spectrum of measured photoacoustic signals to distinguish different liquids [23]. Built upon that mechanism, Zhao *et al.* realized the detection of blood viscosity *in vivo* by analyzing the frequency spectrum of blood photoacoustic signals [24]. The measurement accuracy in these methods, however, are limited by the ultrasonic bandwidth and noise.

Here, we present a new method to measure liquid viscosity in generic microfluidic-based tubes based on the PA Grueneisen relaxation effect [25]. We use a dual-pulse photoacoustic flowmetric method [26] to measure the liquid flow speed in a generic microfluidic-based tube. The average flow speed is inversely proportional to the viscosity. Thus, after calibration, we can determine the viscosity from the flow speed. In the dual-pulse photoacoustic flow measurement, the flow alters the ratio between two PA amplitudes via the Grueneisen relaxation effect. We establish a model between the dual-pulse PA signals and the viscosity in the microfluidic-based tube. Different viscous liquids and blood samples are tested, yielding results that are well consistent with the theoretical values. Experimental results indicate that the proposed method can potentially be a new tool for efficient and convenient liquid viscosity measurement and even be engineered in the future for daily monitoring blood viscosity with only a small amount of blood.

2. Materials and methods

2.1. System setup

Figure 1(a) shows a dual-pulse photoacoustic viscosity measurement platform. A 532-nm laser (7-ns pulse width, VPFL-G-20, Spectra-Physics, USA) serves as the excitation laser pulse source, and its output is separated into two paths by a polarizing beam splitter (PBS1, PBS051, Thorlabs Inc, USA). A half-wave plate (HWP1, GCL-060633, Daheng Optics, China) is placed in front of PBS1 to adjust the energy ratio between the two daughter laser beams. One of the laser beams transmits in free space and the other is coupled into a 30-m single-mode fiber (SMF, HB450-SC, Fibercore, UK), which delays the laser pulse by ~146 ns, as shown in Fig. 1(b). To suppress the stimulated Raman scattering effect in the SMF, another half-wave plate (HWP2, GCL-060633, Daheng Optics, China) is added before the fiber to adjust the polarization state. The pulse energy of each laser beam is ~90 nanojoules. The two beams are recombined by another polarizing beam splitter (PBS2, PBS051, Thorlabs Inc, USA) and coupled into a 2-m single-mode fiber (SM fiber, P1-460B-FC-2, Thorlabs Inc, USA), and then delivered to the scanning PA probe. Light from the 2-m fiber is focused by two achromatic doublets (AC064-013-A, Thorlabs Inc, USA) and excites the sample. The generated photoacoustic signal is received by a piezoelectric ultrasound transducer (UT, V214-BC-RM, Olympus-NDT). The excitation light and acoustic detection are confocally and coaxially aligned to optimize the sensitivity. Detailed information on the probe can be found in our previous publications [27,28]. Driven by a constant pressure produced by an air compressor (JUBA, Yuteng Hardware and Electrical Tech, China), different viscous liquids flow in a transparent circle polyvinyl chloride micro-tube (0.25-mm inner diameter, TYGON S-54- HL, Norton Performance Plastics, China) at different speeds. Considering that the channels of the tube can affect the measurement results [29], we used identical tubes in all experiments. In addition, note that the flow speed at different positions inside the tube is different, leading to different Grueneisen relaxation effects. Thus, in experiment the laser beam was focused onto the same depth of the microtube for all measurements, and same position on the A-line of the generated signals was chosen to extract the PA signal amplitudes for each measurement. The exact temporal position was kept constant all through, making sure PA signals were from the

Biomedical Optics EXPRESS

same depth of the microtube in the study. In other words, the location of the peak-to-peak shape in the A-line of the generated photoacoustic signal for the first sample is marked as the standard position. We then adjust the distance between the excitation laser beams and the tube to ensure that photoacoustic signals from the subsequent targets appear in the identical position.

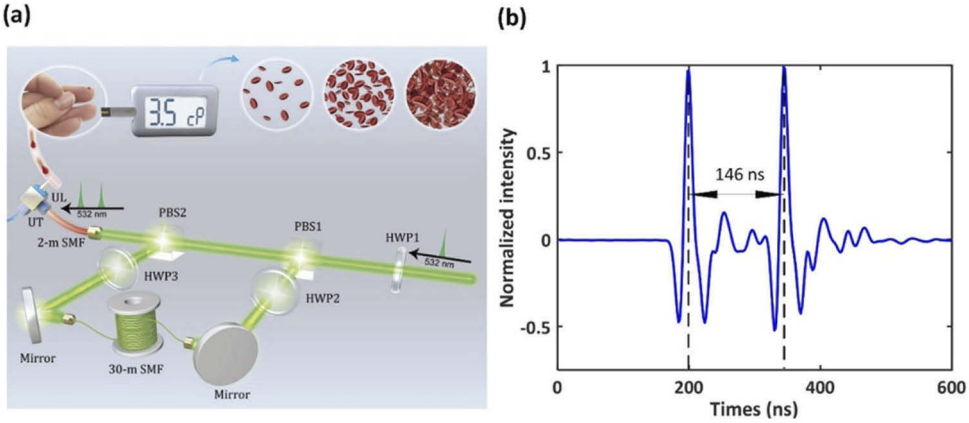

Fig. 1. (a) Schematic of the dual-wavelength photoacoustic viscosity measurement platform. HWP, half-wave plate; PBS, polarizing beam splitter; SMF, single-mode fiber; UL, ultrasound lens; UT, ultrasound transducer. (b) 146-ns time delay between the two optical pulses.

2.2. Sample preparation

Different viscous liquids are obtained by mixing ink solutions with different contents of surfactants solutions (20% Tween 20 aqueous solutions, Scientific Phygene, China). Tween 20 is a polyoxyethylene sorbitol ester containing 20 units of ethylene oxide per unit of sorbitol, which is widely used in microfluidic studies as an oil-in-water (O/W) emulsifier.

Blood samples are bovine whole blood (3.2% sodium citrate added, Hongquan Bio Inc, Guangzhou, China). To mimic anemia and polycythemia conditions, different viscous blood samples are obtained by mixing different concentrations of plasma and hemocytes [11]. In brief, the normal whole blood (~40% haematocrit) is centrifuged at 1400 rpm for 3 minutes to separate the plasma and hemocytes. The upper half is extracted as the plasma and the remaining half as the blood with ~80% haemotocrit. Then, 75% plasma volume and 25% plasma volume are mixed with appropriate hemocytes to mimic anemia (~20% haematocrit) and polycythemia (~60% haematocrit) conditions, respectively. The whole bovine blood is used as the normal group.

Note that the PA viscosity measurement method is based on optical absorption of the target, which is not suitable for clear solutions at 532 nm wavelength. If the viscosity of a transparent solution is to be measured, optical absorbers should be added and stirred with the solution under the condition that the optical absorbers will not alter the viscous performance of the solutions considerably. On the other hand, if the wavelength of the excitation laser can be modified to match the absorption spectrum of the transparent solutions, no additional absorbers will be needed.

2.3. Working principle

Based on Poiseuille's law [30], the flow rate of liquid, Q, in a cylindrical tube is

$$Q = \frac{(P_2 - P_1)\pi r^4}{8\xi l} \tag{1}$$

where P_2 and P_1 are the pressures at the inlet and outlet ends of the tube, r and l are the inner diameter and the length of the tube, and ξ is the liquid viscosity. As the flow rate Q is directly

Biomedical Optics EXPRESS

related to flow speed (v), $Q = \pi r^2 v$, combining with Eq. (1), the liquid viscosity ξ can be expressed as

$$\xi = \frac{(P_2 - P_1)\pi r^4}{8lQ} = \frac{\Delta p r^2}{8lv} \tag{2}$$

The pressure difference (Δp) can be controlled by the air compressor and the parameters (r and l) of the tube are constant. Thus, the liquid viscosity ξ can be calculated from the flow speed v.

The flow speed is obtained based on the dual-pulse photoacoustic platform described above (Fig. 1(a)). In a linear range, the two sequentially excited photoacoustic signals (PA_1 and PA_2) can be written as [31,32]

$$PA_1 = k\Gamma_0 \eta F_1 \mu_a \tag{3}$$

$$PA_2 = k(\Gamma_0 + \Delta\Gamma)\eta F_2 \mu_a \tag{4}$$

where k is the detection sensitivity, Γ_0 is the Grueneisen parameter at the baseline temperature, $\Delta\Gamma$ is the changed Grueneisen parameter due to the first pulse heating effect, η is the coefficient for light-to-heat conversion, F_1 and F_2 are the optical fluences, and μ_a is the optical absorption coefficient. The changed Grueneisen parameter $\Delta\Gamma$ is proportional to the local temperature rise, which can be modeled as [25,33–35]

$$\Delta\Gamma = aF_1\mu_a e^{-(\tau_a + bv)\delta t} \tag{5}$$

where a and b are constant coefficients, τ_a is a constant related to the thermal conduction, v is the flow speed, and δt is the known time delay between the two pulse excitations. As mentioned above, the optical fluences, F_1 and F_2 are the same in our experiment. Thus, the ratio between the second and the first photoacoustic signals can be simplified as

$$Ratio = \frac{PA_2}{PA_1} = \frac{k(\Gamma_0 + \Delta\Gamma)\eta F_2 \mu_a}{k\Gamma_0 \eta F_1 \mu_a} = 1 + \frac{\Delta\Gamma}{\Gamma_0} = 1 + \frac{aF_1\mu_a e^{-(\tau_a + bv)\delta t}}{\Gamma_0} \tag{6}$$

Due to the different thermal properties of the absorption materials, parameter a may be either positive or negative, which means PA_2 can be larger or smaller than PA_1. Taking logarithmic operation on both sides of Eq. (6), we obtain

$$ln(|1 - Ratio|) = -(\tau_a + bv)\delta t + ln\frac{|a|F_1\mu_a}{\Gamma_0} = mv + n \tag{7}$$

where $m = -b\delta t$, and $n = -\delta t\tau_a + ln\frac{|a|F_1\mu_a}{\Gamma_0}$, both of which can be determined via system calibration. Therefore, the flow speed v can be determined from the two PA signals. The liquid viscosity can be calculated from

$$\xi = \frac{\Delta p r^2 m}{8l[ln(|1 - Ratio|) - n]} \tag{8}$$

3. Results and discussion

3.1. System calibration

To obtain the system parameters m and n in Eq. (7), a pure ink sample (no surfactant) was used to calibrate the relationship between the PA 'Ratio' and the preset flow speed. The air compressor in this calibration was removed temporally, and the liquid flow speed was set by a syringe pump within a range from 1 to 25 mm/s. The values of $ln(|1 - Ratio|)$ at different flow speeds are plotted in Fig. 2(a). As expected, the decay constant is approximately a linear function of the flow speed with a determination coefficient (R^2) of 0.97, indicating a strong dependence of the dual-pulse signal ratio on the flow speed. The fitted curve between these two parameters

Biomedical Optics EXPRESS

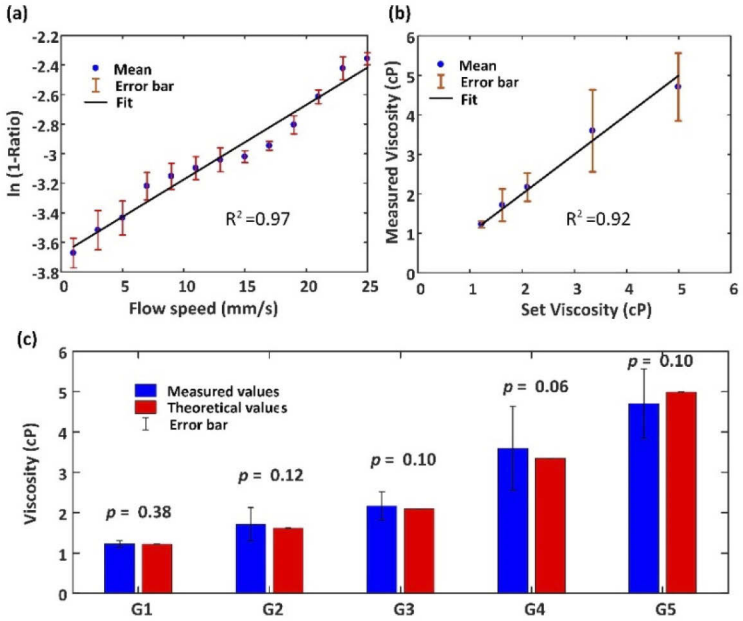

Fig. 2. (a) Ratio between the two PA amplitudes versus the preset set flow speed. Error bars are standard deviations based on 80 measurements. (b) Measured viscosity versus the theoretical set viscosity. (c) Statistical differences between the measured viscosities and theoretical values. G1-G5: Group1-5.

can be expressed by $ln(|1 - Ratio|) = 0.05v - 3.68$, where 0.05 and −3.68 correspond to m and n in Eq. (7), respectively. With the calibration results, the viscosity can be computed from $\xi = \frac{0.05\Delta p r^2}{8l[ln(|1-Ratio|)+3.68]}$.

Because the pressure difference (Δp) and tube parameters (r and l) are constant, we can simplify the relationship between the liquid viscosity and the signal amplitude ratio to $\xi = \frac{c}{ln(|1-Ratio|)+3.68}$, where $c = \frac{0.05\Delta p r^2}{8l}$ is a constant if one type of viscous solution is applied to calibrate the system.

3.2. Phantom viscosity measurement

Next, 90% surfactant-containing solution (with a viscosity coefficient of 7.10 cP) was first used as the calibration sample. The solution flowed in the microfluidic tube under a constant pressure produced from the air compressor. The sample was excited by two sequential laser pulses. The ratio of the two PA signals was computed. The value of c was calculated as 2.72 for the setup. Then, samples of various viscosities (10%, 20%, 30%, 50%, and 70% of surfactant-containing solutions; around 50 µL usage for each sample) were tested under the same pressure. Note that establishing and calibrating the photoacoustic system could be time consuming, and it also takes some time to prepare the samples. When the system and samples are ready, as the repetition rate of the laser pulses was 8 kHz, thus the measurement process can be completed in one dual-pulse excitation. To increase the accuracy, one sample was excited by 10,000 times for averaging. The entire testing takes about 1.25 seconds for one sample flowing in the tube. Considering the injection time and preparing time, the whole process could be finished in several minutes. Based on the experimental results, the viscosity coefficients of these solutions were computed to be 1.22, 1.62, 2.10, 3.35, and 4.99 cP, respectively. These are compared with the theoretical solution viscosities, as shown in Fig. 2(b). The error bar represents the standard deviation based on 80 measurements. The two sets of data are linearly correlated with a determination

Biomedical Optics EXPRESS

coefficient (R^2) of 0.92. We further calculate the statistical differences between the measured and theoretical values for different groups using paired *t-test*, which is shown in Fig. 2(c). The *p*-values indicate no significant differences between the measured values and theoretical values. These demonstrates that the proposed Grueneisen-based dual-pulse PA method can precisely determine the liquid viscosity. Note that higher error bars for more viscous liquids is associated with the nature of the logarithmic operation that amplifies the divergence of measured Grueneisen effect. This point also sets a limitation to the proposed viscosity measurement method, which needs to be measured several times to increase the accuracy.

3.3. Blood viscosity measurement

Since hematocrit is closely related to viscosity, different viscous bovine blood samples were prepared by mixing the hematocrit with different concentrations of plasm as described in Materials and Methods. Each blood sample had a volume around 50 μL and was injected into the microfluidic tube. Then the blood flowed under the same constant pressure as the calibration one. As shown in Fig. 3, the measured blood viscosity results show a good linear relationship with the hematocrit concentrations and agree well with the literatures in which 20% hematocrit (anemia) induces a blood viscosity of $\sim 2 \times 10^{-3} Pa \cdot s$, normal human or bovine blood has a viscosity of $3 - 4 \times 10^{-3} Pa \cdot s$, and the 60% hematocrit (polycythemia) induces a viscosity of $6 - 8 \times 10^{-3} Pa \cdot s$ [36]. The results validate that dual-pulse PA viscosity measurement method can measure viscosity with low blood consumption. Another advantage is that the method is free from any chemical or labelling process. The blood sample can be recollected for retest or other uses, which is meaningful for precious or scarce samples.

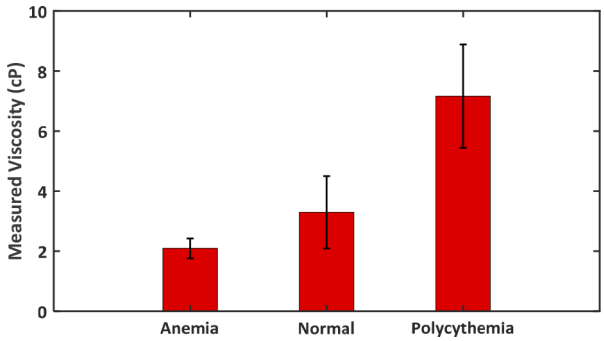

Fig. 3. Comparison of measured viscosity values for different groups of blood samples. The error bar represents the standard deviation based on 25 measurements.

4. Conclusion

In this study, a new method is proposed to measure the liquid viscosity in a generic microtube using a dual-pulse PA platform. An inverse model is developed to quantify the liquid viscosity from two PA signals. We experimentally demonstrate that, with calibration, we can successfully measure the viscosity using only one droplet of liquid/ blood. Note that this dual-pulse PA measurement method uses only regular microtubes, instead of specifically designed supporting structures, greatly reducing the complexity of system design and the operational cost. Moreover, a whole measurement process for one sample only takes less than one minute excluding the time for system and sample preparation, which can be further shortened if necessary. The platform only requires a tiny dosage of the sample (around 50 μL), which is essential for long-term daily viscosity monitoring or precious and scarce samples. Therefore, the proposed dual-pulse PA viscosity measurement method embraces fast detection speed, low consumption, and low cost

Biomedical Optics EXPRESS

in micro tubes. However, higher viscous samples generate larger error bar in our current stage, which is associated with the nature of the logarithmic operation that amplifies the divergence of measured Grueneisen effect. The measured accuracy can be ensured through increasing the measuring times, which can also be further improved with a higher pulse energy laser, less-scattering micro-based tubes and higher consistent pressure coming from the air compressor. Overall, this is only a proof-of-concept study to demonstrate the principle and feasibility of the proposed PA method; in the future, the system will be further engineered to increase the accuracy till it can be directly compared with other advanced equipment or methods. From a long-term aspect, it opens a new venue for efficient microfluidic-based liquid viscosity measurement and this platform may potentially be engineered into a small point-of-care device with tiny lasers and fibers to test the blood viscosity in the future, which would benefit a large population of patients with abnormal blood viscosities.

Appendix

The spectrum of the excitation beams

In order to ensure the same wavelengths for the two excitations beams, the spectrum of the excitations beams were tested using spectrometer and the result is shown in Fig. 4. Only one peak wavelength of 532 nm is observed, which indicates that the stimulated Raman scattering (SRS) effect is suppressed.

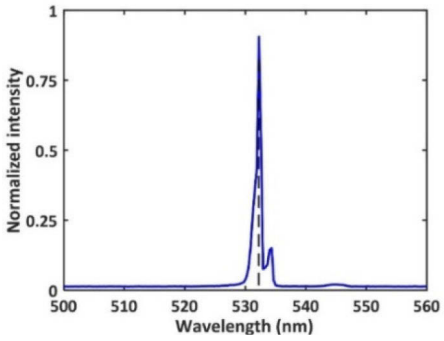

Fig. 4. The spectrum of the excitation beam (including two paths), showing a sole wavelength of 532 nm.

Regular PA signals from phantoms

A batch of well mixed solutions of different viscosities are shown in Fig. 5(a). To investigate if the regular (single-beam) PA signal significantly depends on the concentration of surfactant, different solutions were measured and compared under the same conditions. All solutions were injected into the microfluidic tube without flowing and excited by one laser pulse. The pulse energy was ~90 nanojoules, and the pulse repetition rate was 8 kHz. As shown in Fig. 5(b), the single-beam photoacoustic signal amplitude changes very slightly with the contents of surfactants. The peak-to-peak amplitudes are extracted and shown in Fig. 5(c). As seen, compared with the solution containing 10% surfactants, the single-beam PA signal amplitude of the 70% solution only reduces by ~2.78%, and the signal amplitudes of the 50%, 30%, and 20% solutions drop by merely about 2.59%, 1.89%, and 0.90%, respectively. The result suggests that the difference of the surfactant concentration and the liquid viscosity induces very limited variation to the optical absorption coefficient of the solution and hence the single-beam PA signal strength. Moreover, the small divergences, if exist, can be easily compensated based on the measured results.

Biomedical Optics EXPRESS

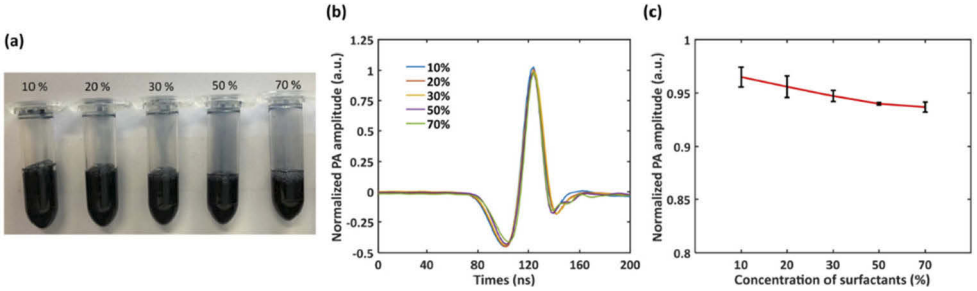

Fig. 5. (a) Photograph of surfactant-ink solutions of different viscosities (containing 10%, 20%, 30%, 50% and 70% of surfactant, respectively). (b) Normalized PA signals of different surfactant-ink solutions. (c). PA signal (peak to peak) amplitude as a function of surfactant concentration.

Dual-pulse PA signals and liquid viscosity

After confirming the small absorption fluctuations caused by different concentrations of surfactants, solutions were injected in turns and flowed in the microfluidic tube under a constant pressure driven by the air compressor. Measurements were performed with the dual-pulse PA setting as described above. For each group of solutions, dual-pulse PA signals, as illustrated in Fig. 6(a), were obtained. As seen, the two PA signals corresponding to the two pulses can be easily distinguished and separated. The peak-to-peak values of the second and the first photoacoustic signals are extracted, and the ratio between them is defined as 'Ratio'. The values of $ln(|1 - Ratio|)$ at different surfactant concentrations are plotted in Fig. 6(b). As seen, the measured logarithm value shows an inverse proportional trend with the solution concentration. This is consistent with the fitted curve derived based on Eqs. (7) and (2), which follows a relation $ln(|1 - Ratio|) = \frac{24.26}{con} - 3.51$ with a determination coefficient (R^2) of 0.97, where *con* is the surfactant concentration. This result, again, confirms the feasibility of the proposed dual-pulse PA method for viscosity measurement.

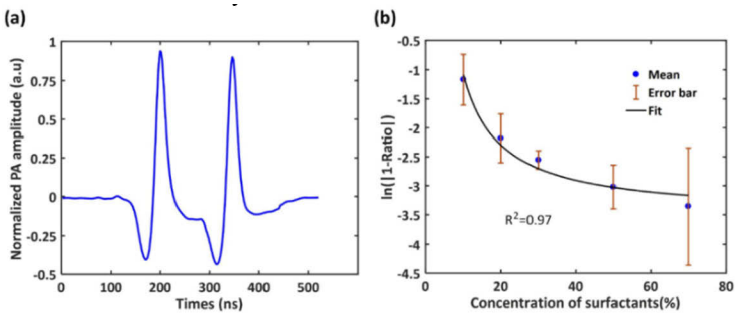

Fig. 6. (a) A representative dual-pulse PA signal. (b) The value of $ln(|1 - Ratio|)$ versus the surfactant concentration. Error bars are standard deviation based on 80 measurements.

Funding. Hong Kong Innovation and Technology Commission (GHP/043/19SZ, GHP/044/19GD, ITS/022/18); Hong Kong Research Grant Council (11101618, 11103320, 11215817, 15217721, 21205016, 25204416, R5029-19); National Natural Science Foundation of China (81627805, 81671726, 81930048); Guangdong Science and Technology Commission (2019A1515011374, 2019BT02X105); Science, Technology and Innovation Commission of Shenzhen Municipality (JCYJ20160329150236426, JCYJ20170413140519030, JCYJ20170818104421564, SGDX20190917094601717).

Acknowledgments. The authors thank Jiyu Li of The City University of Hong Kong for offering the microfluidic system for detection. This work was partially supported by the National Natural Science Foundation of China (NSFC) (81930048, 81671726, 81627805), Guangdong Science and Technology Commission (2019BT02X105,

Biomedical Optics EXPRESS

2019A1515011374), Hong Kong Innovation and Technology Commission (GHP/043/19SZ, GHP/044/19GD, ITS/022/18), and Hong Kong Research Grant Council (15217721, R5029-19, 25204416, 21205016, 11215817, 11101618, 11103320), and Shenzhen Science and Technology Innovation Commission (SGDX20190917094601717, JCYJ20170818104421564, JCYJ20160329150236426, JCYJ20170413140519030).

Disclosures. L.W. has a financial interest in PATech Limited, which, however, did not support this work.

Data availability. Data underlying the results presented in this paper are not publicly available at this time but may be obtained from the authors upon reasonable request within 5 years after publication date.

References

1. R. Rosencranz and S. A. Bogen, "Clinical laboratory measurement of serum, plasma, and blood viscosity," Am J Clin Pathol **125**(suppl_1), S78–S86 (2006).
2. B. Jakoby, M. Scherer, M. Buskies, and H. Eisenschmid, "An automotive engine oil viscosity sensor," Ieee Sens J **3**(5), 562–568 (2003).
3. G. D. O. Lowe, M. M. Drummond, A. R. Lorimer, I. Hutton, C. D. Forbes, C. R. M. Prentice, and J. C. Barbenel, "Relation between extent of coronary-artery disease and blood-viscosity," Brit Med J **280**(6215), 673–674 (1980).
4. G. D. O. Lowe, F. G. R. Fowkes, J. Dawes, P. T. Donnan, S. E. Lennie, and E. Housley, "Blood-viscosity, fibrinogen, and activation of coagulation and leukocytes in peripheral arterial-disease and the normal population in the edinburgh artery study," Circulation **87**(6), 1915–1920 (1993).
5. S. Shin and D. Y. Keum, "Measurement of blood viscosity using mass-detecting sensor," Biosens Bioelectron **17**(5), 383–388 (2002).
6. Y. J. Kang, J. Ryu, and S. J. Lee, "Label-free viscosity measurement of complex fluids using reversal flow switching manipulation in a microfluidic channel," Biomicrofluidics **7**(4), 044106 (2013).
7. H. Kim, Y. I. Cho, D. H. Lee, C. M. Park, H. W. Moon, M. Hur, J. Q. Kim, and Y. M. Yun, "Analytical performance evaluation of the scanning capillary tube viscometer for measurement of whole blood viscosity," Clin Biochem **46**(1-2), 139–142 (2013).
8. W. J. Lan, S. W. Li, J. H. Xu, and G. S. Luo, "Rapid measurement of fluid viscosity using co-flowing in a co-axial microfluidic device," Microfluid Nanofluid **8**(5), 687–693 (2010).
9. S. Kim, K. C. Kim, and E. Yeom, "Microfluidic method for measuring viscosity using images from smartphone," Opt Laser Eng **104**, 237–243 (2018).
10. Y. J. Kang, S. Y. Yoon, K. H. Lee, and S. Yang, "A highly accurate and consistent microfluidic viscometer for continuous blood viscosity measurement," Artif Organs **34**(11), 944–949 (2010).
11. L. Liu, D. Hu, and R. H. W. Lam, "Microfluidic viscometer using a suspending micromembrane for measurement of biosamples," Micromachines (Basel) **11**(10), 934 (2020).
12. L. H. V. Wang and S. Hu, "Photoacoustic tomography: in vivo imaging from organelles to organs," Science **335**(6075), 1458–1462 (2012).
13. Y. Zhou, J. Chen, C. Liu, C. Liu, P. Lai, and L. Wang, "Single-shot linear dichroism optical-resolution photoacoustic microscopy," Photoacoustics **16**, 100148 (2019).
14. P. Lai, L. Wang, J. W. Tay, and L. V. Wang, "Photoacoustically guided wavefront shaping for enhanced optical focusing in scattering media," Nat Photonics **9**(2), 126–132 (2015).
15. X. Huang, W. Shang, H. Deng, Y. Zhou, F. Cao, C. Fang, P. Lai, and J. Tian, "Clothing spiny nanoprobes against the mononuclear phagocyte system clearance in vivo: Photoacoustic diagnosis and photothermal treatment of early stage liver cancer with erythrocyte membrane-camouflaged gold nanostars," Applied Materials Today **18**, 100484 (2020).
16. H. Li, F. Cao, Y. zhou, Z. yu, and P. Lai, "Interferometry-free noncontact photoacoustic detection method based on speckle correlation change," Opt. Lett. **44**(22), 5481–5484 (2019).
17. Z. P. Yu, H. H. Li, and P. X. Lai, "Wavefront shaping and its application to enhance photoacoustic imaging," Appl Sci-Basel **7**(12), 1320 (2017).
18. F. Cao, Z. Qiu, H. Li, and P. Lai, "Photoacoustic imaging in oxygen detection," Appl. Sci. **7**(12), 1262 (2017).
19. Y. Wang, Y. Zhan, M. Tiao, and J. Xia, "Review of methods to improve the performance of linear array-based photoacoustic tomography," J. Innovative Opt. Health Sci. **13**(02), 2030003 (2019).
20. C. Liu, J. B. Chen, Y. C. Zhang, J. Y. Zhu, and L. D. Wang, "Five-wavelength optical-resolution photoacoustic microscopy of blood and lymphatic vessels," Adv Photonics **3**(01), 016002 (2021).
21. X. Chen, W. Qi, and L. Xi, "Deep-learning-based motion-correction algorithm in optical resolution photoacoustic microscopy," Vis Comput Ind Biomed Art **2**(1), 12 (2019).
22. Y. Ma, C. Lu, K. Xiong, W. Zhang, and S. Yang, "Spatial weight matrix in dimensionality reduction reconstruction for micro-electromechanical system-based photoacoustic microscopy," Vis. Comput. Ind. Biomed. Art **3**(1), 22 (2020).
23. C. G. Lou and D. Xing, "Photoacoustic measurement of liquid viscosity," Appl. Phys. Lett. **96**(21), 211102 (2010).
24. Y. Zhao, S. Z. Yang, Y. T. Wang, Z. Yuan, J. L. Qu, and L. W. Liu, "In vivo blood viscosity characterization based on frequency-resolved photoacoustic measurement," Appl. Phys. Lett. **113**(14), 143703 (2018).
25. L. Wang, C. Zhang, and L. V. Wang, "Grueneisen relaxation photoacoustic microscopy," Phys. Rev. Lett. **113**(17), 174301 (2014).
26. C. Liu, Y. Liang, and L. Wang, "Single-shot photoacoustic microscopy of hemoglobin concentration, oxygen saturation, and blood flow in sub-microseconds," Photoacoustics **17**, 100156 (2020).

Biomedical Optics EXPRESS

27. Y. Zhou, S. Liang, M. Li, C. Liu, P. Lai, and L. Wang, "Optical-resolution photoacoustic microscopy with ultrafast dual-wavelength excitation," J. Biophotonics **13**(6), e201960229 (2020).
28. L. D. Wang, K. Maslov, J. J. Yao, B. Rao, and L. H. V. Wang, "Fast voice-coil scanning optical-resolution photoacoustic microscopy," Opt. Lett. **36**(2), 139–141 (2011).
29. J. Zhou and I. Papautsky, "Viscoelastic microfluidics: progress and challenges," Microsyst. Nanoeng. **6**(1), 113 (2020).
30. J. Pfitzner, "Poiseuille and his law," Anaesthesia **31**, 273–275 (1976).
31. M. H. Xu and L. H. V. Wang, "Photoacoustic imaging in biomedicine," Rev. Sci. Instrum. **77**(4), 041101 (2006).
32. W. H. L. V. Wang, "Biomedical optics: principles and imaging," in *Biomedical Optics*, 362 (Wiley, 2007), pp. 283–321.
33. L. D. Wang, J. J. Yao, K. I. Maslov, W. X. Xing, and L. H. V. Wang, "Ultrasound-heated photoacoustic flowmetry," J. Biomed. Opt **18**(11), 117003 (2013).
34. A. Sheinfeld and A. Eyal, "Photoacoustic thermal diffusion flowmetry," Biomed. Opt. Express **3**(4), 800–813 (2012).
35. W. Liu, B. X. Lan, L. Hu, R. M. Chen, Q. F. Zhou, and J. J. Yao, "Photoacoustic thermal flowmetry with a single light source," J Biomed Opt **22**(9), 096001 (2017).
36. M. S. Litwin and K. Chapman, "Physical factors affecting human blood viscosity," J. Surg. Res. **10**(9), 433–436 (1970).